Nuclear Instruments and Methods in Physics Research B 268 (2010) 254–258

Contents lists available at ScienceDirect

Nuclear Instruments and Methods in Physics Research B

journal homepage: www.elsevier.com/locate/nimb

# XBIC/μ-XRF/μ-XAS analysis of metals precipitation in block-cast solar silicon

M. Trushin [a,*], W. Seifert [a,b], O. Vyvenko [b,c], J. Bauer [d], G. Martinez-Criado [e], M. Salome [e], M. Kittler [a,b]

[a] IHP/BTU Joint Lab, Konrad-Wachsmann-Allee 1, 03046 Cottbus, Germany
[b] IHP Microelectronics, Im Technologiepark 25, 15236 Frankfurt (Oder), Germany
[c] V.A. Fok Institute of Physics, St. Petersburg State University, Ulyanovskaya 1, 108594 St. Petersburg, Russia
[d] Max Planck Institute of Microstructure Physics, Weinberg 2, 06120 Halle, Germany
[e] ESRF, 6 rue Jules Horowitz, 38043 Grenoble Cedex, France

ARTICLE INFO

*Article history:*
Received 1 June 2009
Received in revised form 30 August 2009
Available online 13 October 2009

*Keywords:*
Silicon
Defects
Metal precipitates
Nucleation sites
XRF
XAS

ABSTRACT

The results of the investigations of the interaction between the different impurities in intentionally contaminated block-cast multi-crystalline silicon by means of synchrotron-based microprobe techniques XBIC (X-ray beam induced current), μ-XRF (X-ray fluorescence microscopy) and μ-XAS (X-ray absorption microspectroscopy) recently implemented at beamlines ID-21 and ID-22 of ESRF, Grenoble, are presented. It was found that $Si_3N_4$/SiC particles frequently observed in the upper part of multi-crystalline Si blocks represent effective sinks for Fe and Cu impurities. The amount of precipitated iron was the same order magnitude both at nitride and carbide particles. The amount of Cu precipitated at the SiC inclusions was significantly larger than that at $Si_3N_4$ rods. Chemical state of the copper precipitates was identified as copper-rich silicide $Cu_3Si$. The anneal at 950 °C that is known to enhance oxygen precipitation in silicon was found to accompany with the enhanced formation of nanoscale iron disilicide precipitates both inside the grains and at grain boundaries.

© 2009 Elsevier B.V. All rights reserved.

## 1. Introduction

The electrical properties of cost-effective multi-crystalline silicon (mc-Si) materials for solar cell applications are strongly affected by extended crystal defects and impurities, in particular by transition metals. Being widely distributed, copper and iron are particularly harmful. These metals could be introduced into mc-Si wafers from the feedstock during the crystal growth or could penetrate from the wafer surface into the bulk during any heat treatment. Their concentration was found to be as high as $10^{14}$–$10^{16}$ $cm^{-3}$ in most mc-Si materials [1].

Fortunately, the presence of such high metal content in mc-Si does not necessarily mean a poor material quality. The impact of transition metals on the solar cell efficiency depends strongly on their particular state inside the Si lattice, i.e. whether they are homogeneously solved or locally concentrated in precipitates [2]. Obviously, the big and rarely spaced precipitates will be less harmful for device yield than the small and dense clusters [3,4]. mc-Si contains various types of defects such as grain boundaries (GB), dislocations, precipitates and inclusions of foreign phases that can serve generally as the sites for metals precipitation. However, the question which kinds of defects are the most preferable sinks for the transition metals is open so far. Accordingly, new data about the processes of transition metal interaction with structural defects in mc-Si are needed to find paths for further improvement of solar cell performance.

It was demonstrated previously [5,6] that the combination of the synchrotron-based analysis techniques X-ray beam induced current (XBIC), X-ray fluorescence microscopy (μ-XRF) and X-ray absorption microspectroscopy (μ-XAS) could provide highly needed spatially resolved information about the sizes, distribution and chemical state of metal-rich particles inside the silicon matrix. μ-XRF mapping is applied to detect and characterize the elemental compositions, sizes and depths of metal-rich clusters by means of recording the characteristic X-ray fluorescence radiation produced by the incoming focused X-ray beam. The X-ray beam induced current (XBIC) technique is used to determine the recombination activity of defects in a way similar to electron/laser beam induced current techniques (EBIC and LBIC, respectively): the incoming X-ray beam generates electron–hole pairs, and minority carrier current is collected then by a space charge region of a Schottky diode [5]. At last, X-ray absorption microspectroscopy (μ-XAS) technique helps to determine the chemical state of the metal-rich particles detected by μ-XRF mapping [2].

Previously we found different behavior of copper and iron with respect to the oxygen precipitates and grain boundaries [7,8]:

* Corresponding author. Tel.: +49 0355 69 3904; fax: +49 0355 69 4961.
*E-mail address:* trushmax@tu-cottbus.de (M. Trushin).

0168-583X/$ - see front matter © 2009 Elsevier B.V. All rights reserved.
doi:10.1016/j.nimb.2009.09.057

while copper readily precipitated both at the precipitates and grain boundaries, iron segregation was observed preferentially at grain boundaries. Here we report our latest results about the interaction of Cu and Fe impurities with silicon nitride $Si_3N_4$ and silicon carbide SiC particles as well as about Fe precipitation in mc-Si stimulated by oxygen. Also, technical specifications and limitations of the two synchrotron beamlines used for this study will be shortly discussed.

## 2. Analytical techniques

The synchrotron-based X-ray microprobe techniques were carried out at the beamlines ID-21 and ID-22 of ESRF, Grenoble. Beamline ID-21 provides X-ray source with the energies up to 7.5 keV giving access to the iron absorption edge but not to that of copper. Our measurements were performed in a vacuumed chamber in order to reduce the background signal due to the scattering of the exciting X-ray beam in the air. The beam was focused with zone plate optics to the spot size of 0.25 μm × 1.5 μm with the photon flux of about few of $10^9$ photons/s enabling the detection of iron-reach clusters of sub-micron sizes.

At the "high energy" beamline ID-22 the X-ray beam energy was set at 9.5 keV to allow the detection of all relevant metals up to copper. Measurements were carried out in air. Kirkpatrick-Baez mirror focusing system was adjusted to achieve X-ray spot size of 3.5 μm × 1.5 μm on the sample surface, at a peak flux of a few $10^9$ photons/s.

To detect the outcoming X-ray fluorescence silicon drift detector at ID-21 and 13-element Si(Li) detector at ID-22 were employed, while Keithley 6485 picoamperemeters were used to register XBIC signals. Sample stage systems of the both beamlines allow precise positioning of the sample in vertical and horizontal directions with accuracy better than 0.1 μm.

Firstly, fast XBIC scans in continuous mode or with a large step size (up to tens of microns) were performed to find the regions with enhanced recombination activity. The shortest dwell time of the set-ups was used in this case that was limited by the response time of the mechanical system only (typically ~0.3 s). Then, in the selected regions, the XBIC/XRF scans with sufficient long acquisition time (typically 1–2 s) were carried out with the step size that was adjusted to the spot size of the beam to cover the investigated area of the sample completely.

After the precipitate images were obtained in XRF-maps, μ-XAS spectra at the absorption edge (XANES) were taken at the points of interest. The XRF-signal from the metal foils of known thickness served as the reference. The total number of the counts of the energy dispersive detectors in a certain energy interval around the Kα-line was taken as the measure of the metal content.

EBIC investigations in a scanning electron microscope served as the pre-characterization step for all synchrotron analyses.

## 3. Samples description

Two different sets of mc-Si samples were used in our study. The first one was p-type mc-Si wafers cut from the near-cap region of the cast block intentionally contaminated with 2 ppma Fe and 20 ppma Cu during the growth. Neutron activation analysis revealed Fe and Cu in concentrations of about $10^{15}$ $cm^{-3}$ and of about $2 \times 10^{16}$ $cm^{-3}$, respectively in such samples.

Besides grain boundaries and dislocations, SiC and $Si_3N_4$ particles were found in the samples. According to the infrared transmission microscopy data $Si_3N_4$ particles had the form of rods or of filaments whereas SiC formed big clusters in the vicinity of $Si_3N_4$ rods. After etching the samples in HF:$HNO_3$ based solution, these particles revealed themselves easily due to their chemical resistance and thus yielded to further analysis in this work. One from these samples was subjected to the synchrotron measurements at the ID-22 beamline.

The samples of the second set were sister wafers of initially non-contaminated cast mc-Si. The wafers were intentionally contaminated from a surface source by iron in-diffusion at 1150 °C for 30 min in high-purity Ar atmosphere terminated by a moderate quench (estimated cooling rate 5 K/s). The remaining metal layer was removed by etching after the contamination treatment. Then the samples were subjected to additional thermal treatments at temperatures of 850 °C, 950 °C and 1050 °C for 16 h to stimulate the precipitate formation. These samples were studied at the ID-21 beamline.

Thin Al layer was evaporated on the chemically polished front surface of all samples to produce Schottky contact for EBIC and XBIC measurements. Ohmic contacts were made by rubbing of InGa eutectic on the rear sample side.

## 4. Experimental results

Fig. 1 represents the EBIC image of the sample of the first set. The main features of the image are Y-shaped solid lines that are unambiguously correspond to grain boundaries, numerous small dark spots in intragranular regions and two large triangular dark spots located at the right grain boundary. The position of the small dark spots were found to coincide well with the position of $Si_3N_4$ particles (rods) observed by IR microscopy. The large triangular dark spots at GB were identified as SiC clusters (inclusions) with a minor addition of silicon nitride.

The regions that are marked by rectangles "a" and "b" in Fig. 1 were chosen for X-ray microscopy analysis. The region "a" contains intragranular $Si_3N_4$ rods and the part of grain boundary. The feature of interest in the region "b" is a large SiC-rich inclusion.

Fig. 2-Cu and Fig. 2-Fe represent XRF-maps of Cu-Ka and of Fe-Ka distributions in the region "a". At least three Cu- and Fe-rich spots can be clearly recognized indicating the presence of the metal precipitates. The positions of detected Fe and Cu precipitates coincide to each other and correspond well to the dark spots on the EBIC image (as well as on XBIC-image that is not shown for brevity), and thus, to the positions of $Si_3N_4$ rods.

The intensities of Cu-Ka and Fe-Ka signals in the precipitates as well as their sizes (typically from 20 × 10 $\mu m^2$ to 5 × 5 $\mu m^2$) were nearly the same. These results showed that $Si_3N_4$ rods gathered

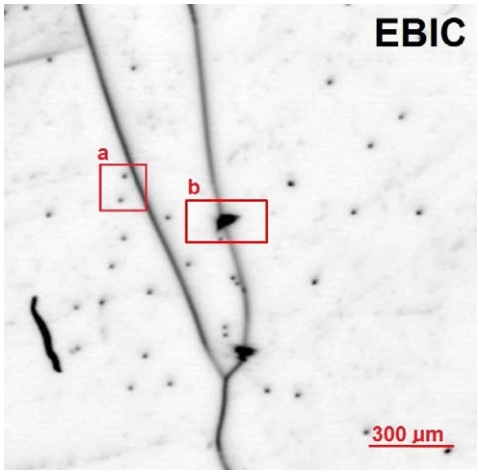


**Fig. 1.** Survey EBIC image of the defects in the Fe/Cu contaminated cast mc-Si sample.

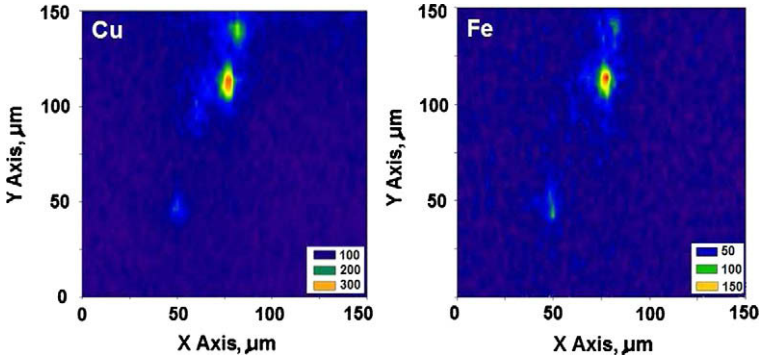


**Fig. 2.** XRF map for Cu-Ka (left) and Fe-Ka (right) taken in the region marked by rectangle "a" in Fig. 1. X-ray fluorescence intensity scales are shown in the legends.

nearly equal amounts of Fe and Cu despite of 1:20 ratio of their total concentrations in silicon wafer.

Fig. 3 depicts XBIC/Cu-Ka/Fe-Ka maps for the region "b" in EBIC image of Fig. 1. A large Cu cluster with small traces of Fe was detected just at the position of the large dark spot in XBIC-image that corresponds to the SiC-rich inclusion. In opposite to the case just described above the ratio of Cu-Ka to Fe-Ka counts was about 200:1, i.e. the copper ratio at SiC cluster exceeded its average ratio by the factor of ten. The results of XANES measurement identified this copper particle as copper silicide, $Cu_3Si$ – see Fig. 4. The chemical composition of the iron particles was not determined due to insufficient intensity of the XRF signal at Fe-Ka absorption edge.

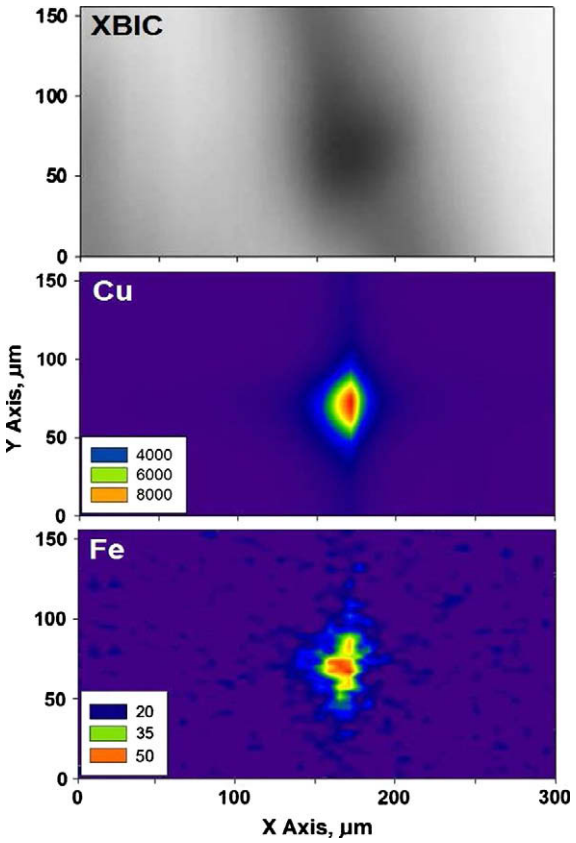


**Fig. 3.** XBIC image and XRF maps for Cu-Ka and Fe-Ka taken in the region marked by rectangle "b" in Fig. 1. Note the difference between the shapes of EBIC (Fig. 1) and XBIC (Fig. 3) contrasts. It is believed due to significant difference in the penetration depth for electrons (6 μm) and for X-ray (60 μm) in Si/SiC. XRF intensity scales are shown in the legends.

Finally, one should note that the concentrations of the metals in all other parts of the samples that did not contain $Si_3N_4$ or SiC particles (including the grain boundaries) were below detection limit of our measurements.

The results obtained on the second sample set are presented in Figs. 5 and 6. No Fe precipitates were detected in the iron as-contaminated samples before the additional thermal treatments as well as after the treatment at 1050 °C. The most pronounced effect of the annealing was registered for the temperature of 950 °C. In this sample Fe-rich precipitates were detected both inside the grains and at grain boundaries. The most of the precipitates were of sub-micron sizes and were collected at the boundaries in colonies that can be seen on the XBIC and XRF maps presented in the Fig. 5. XANES spectra of these iron-related particles were found to be in close agreement with that of iron disilicide $FeSi_2$, see [8] for details. Non-symmetrical shape of the XRF-particles images (with a larger extension in one direction) is due to the elliptical shape of the beam spot (1.5 μm × 0.25 μm).

Only faint traces of Fe clusters were detected in the sample annealed at 850 °C. They were located mostly at the positions where GB changed its direction (compare XBIC and XRF images in Fig. 6).

## 5. Discussion and summary

Our results obtained on the first set of the samples clearly indicated that the silicon carbide and silicon nitride particles represent preferable sites for the metal precipitation. Besides, the precipitation behaviour of Cu and Fe differs significantly with respect to silicon carbide and to silicon nitride.

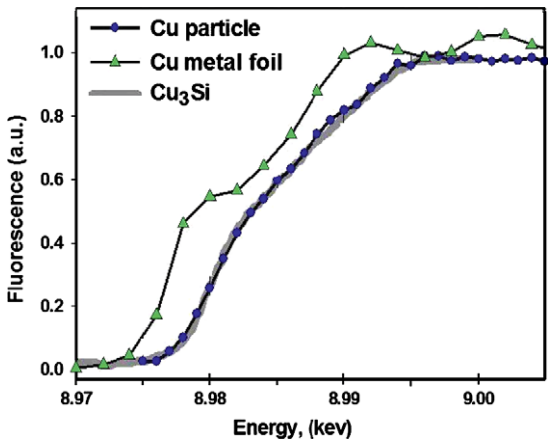


**Fig. 4.** μ-XANES spectrum of the Cu particle from the Fig. 3, compared with the spectrum of copper foil and with the $Cu_3Si$ standard.

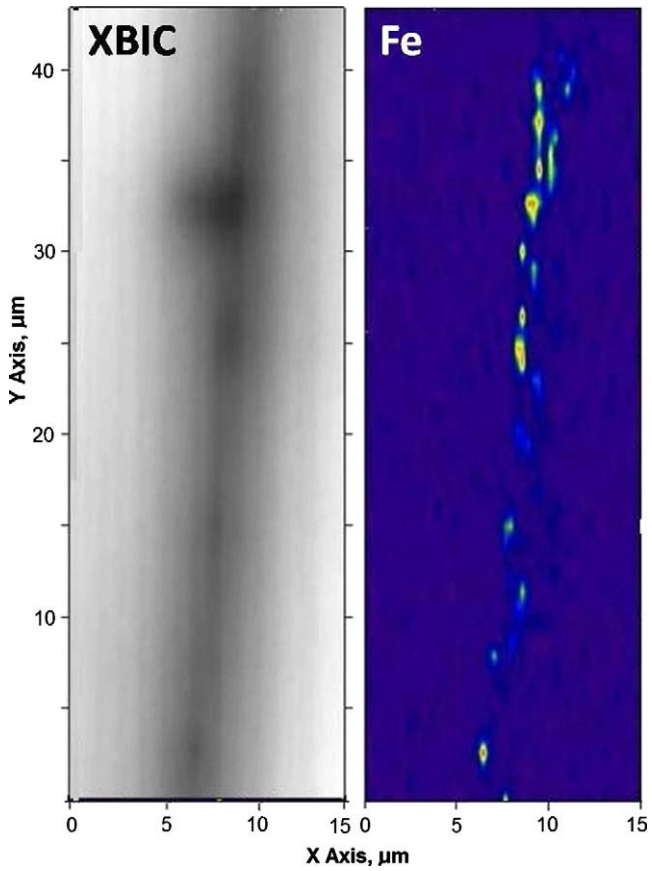


**Fig. 5.** XBIC (right) and Fe (left) maps of the Fe contaminated sample annealed at 950 °C.

It was found that Cu XRF-intensity at the SiC inclusion was nearly 30 times higher than that at $Si_3N_4$ filaments (compare Cu-Ka counts in Fig. 3 in Fig. 2). Since the apparent sizes of Cu-rich region at the particles were larger than the spot size of X-ray beam, this result might be due to corresponding difference in the effective thicknesses of the copper-rich regions around two types of the particles. As it is well known, Cu-rich silicide in form $Cu_3Si$, having a much larger molecular cell volume than that of Si, prefer to precipitate at the extended defects with such local strain fields around them that reduce the nucleation barrier for precipitation [9]. So the origin of enhanced Cu precipitation at the SiC particle might be explained by the larger value and the size of strain fields around the big silicon carbide inclusion as compared with that around small nitride rods.

The intensity of Fe-XRF signal was found to be independent on the Cu amount and was larger at the nitride rods that at the carbide particles. This indicates a minor interaction of iron with copper during precipitation process. This property of iron is in variance with the strong interaction of nickel with copper recently observed in [7] and gives us argument for the conclusion that iron precipitation mechanism differs quantitatively from that of nickel.

The enhanced interaction of iron with silicon nitride rods was previously reported for the similar mc-Si material that was not intentionally contaminated [10]. This fact was explained [10] by the widely used property of iron to be a catalyst in the production of silicon nitride [11]. According to [11], β-$Si_3N_4$ phase growth is defined by the precipitation inside the $FeSi_x$ liquid containing dissolved nitrogen from the vapour. Similar reaction was proposed for precipitates growth in silicon [10,12] assuming the creation iron silicide liquid droplets as the source for the further $Si_3N_4$ growth.

It was found previously (see [13] and references therein), that the presence of iron in silicon led to enhanced precipitation of oxygen after thermal treatment around 950 °C whereas oxygen precipitation both at lower and at higher temperatures was not observed. On the samples of the second set we found that the treatment just at 950 °C has led to particularly strong Fe precipitation. This result confirmed another particular role of iron silicide in precipitation processes in silicon.

The temperature of the enhanced growth of oxygen precipitates [13] as well as of iron silicide precipitates formation found in this work is very close to the eutectoid temperature of α-$FeSi_2$ – 960 °C [14] that is well below silicon melting point. This implies that above this temperature α-$FeSi_2$ droplets remain liquid and might enhance any precipitate ripening by soli-liquid segregation according to the model suggested in [12].

Possibly, the same self-organizing processes take place in our two sets of samples: firstly, the nucleation of iron-silicide clusters-embryos, which serve as sinks for oxygen or nitrogen. At the second stage, the subsequent growth of oxygen precipitates or $Si_3N_4$ particles takes place. These particles, in turn, serve as the sites for further iron gettering giving rise to production of the second generation of iron-silicide embryos and so on.

Measurements of intentionally contaminated mc-Si samples proved that synchrotron-based analysis is a valuable tool to analyze the interaction of metal impurities with crystal defects. The results obtained clearly demonstrate that combined synchrotron-based analysis of electrical activity and metals in solar-grade silicon is operational at ESRF beamlines ID-21 and ID-22. Technical potentials of ID-21 beamline allow studying and analyze of sub-micron iron precipitates with the radius as small as 40 nm. On the other hand, ID-22 beamline can be applied for the investigation of the heavier metals precipitates – such as copper, but

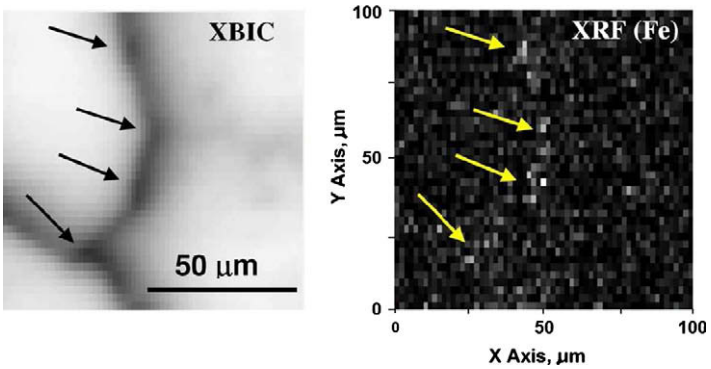


**Fig. 6.** XBIC (left) and Fe (right) maps of the sample annealed the 850 °C. A faint trace of Fe is revealed, mainly at the sites where GB changes its direction (see positions marked by arrows).

due to a larger X-ray spot size it is expedient to use it for the studying of larger sized precipitates at the big area scans. It should be pointed out that the sub-micron size Fe precipitates in our second sample set we were able to investigate only making use the facility of ID-21 beamline. Such small precipitates can not be detected at ID-22 due to significantly larger size of X-ray beam spot with respect to their own sizes, i.e. only a small part of the incident radiation hit the particles.

On the contrary, beamline ID-22 being equipped with Kirkpatrick-Baez mirror focusing system provides a very stable spot position on the sample surface independently on the exciting energy enabling to obtain stable results of spectral absorption. The measurements of sub-micron particles making use zone plate optics of ID-21 may be complicated due systematic shift of the spot position on the nanometer scale caused by the X-ray beam energy variation [8].

## Acknowledgements

The authors acknowledge ESRF Grenoble for provision of synchrotron beamtime. This work was financially supported by the German Federal Ministry for the Environment, Nature Conservation and Nuclear Safety. The content of this publication is the responsibility of the authors.

## References

[1] T. Buonassisi, A.A. Istratov, M.D. Pickett, M. Heuer, J.P. Kalejs, G. Hahn, M.A. Marcus, B. Lai, Z. Cai, S.M. Heald, T.F. Ciszek, R.F. Clark, D.W. Cunningham, A.M. Gabor, R. Jonczyk, S. Narayanan, E. Sauar, E.R. Weber, Prog. Photovolt: Res. Appl. 14 (2006) 513–531.
[2] S.A. McHugo, A.C. Thompson, A. Mohammed, G. Lamble, I. Perichaud, S. Martinuzzi, M. Werner, M. Rinio, W. Koch, H.-U. Hoefs, C. Haessler, J. Appl. Phys. 89 (2001) 4282.
[3] M. Trushin, O. Vyvenko, M. Seibt, Sol. St. Phenom. 131–133 (2007) 155.
[4] M. Kittler, J. Lärz, W. Seifert, M. Seibt, W. Schröter, Appl. Phys. Lett. 58 (9) (1991) 911.
[5] O.F. Vyvenko, T. Buonassisi, A.A. Istratov, H. Heislmair, A.C. Thompson, R. Schindler, E.R. Weber, J. Appl. Phys. 91 (2002) 3614.
[6] T. Buonassisi, A.A. Istratov, M.A. Markus, M. Heuer, M.D. Pickett, B. Lai, Z. Cai, S.M. Heald, E.R. Weber, Sol. St. Phenom. 108–109 (2005) 577.
[7] M. Trushin, O. Vyvenko, W. Seifert, M. Kittler, I. Zizak, A. Erko, M. Seibt, C. Rudolf, Phys. Status Solidi C 6 (8) (2009) 1868.
[8] W. Seifert, O. Vyvenko, T. Arguirov, M. Kittler, M. Salome, M. Seibt, M. Trushin, Superlatt. Microstruct. 45 (2009) 168–176.
[9] A.A. Istratov, E.R. Weber, J. Electrochem. Soc. 149 (1) (2002) G21–G30.
[10] J.P. Rakotoniaina, O. Breitenstein, M. Werner, M. Hejjo Al Rifai, T. Buonassisi, M.D. Pickett, M. Ghosh, A. Müller, N. Le Quang, in: W. Palz, H. Ossenbrink, P. Helm (Eds.), Proc. 20th European Photovoltaic Solar Energy Conference and Exhibition, 2005, pp. 773–776.
[11] S.M. Boyer, A.J. Moulson, J. Mater. Sci. 13 (1978) 1637.
[12] T. Buonassisi, M. Heuer, A.A. Istratov, M.D. Pickett, M.A. Marcus, B. Lai, Z. Cai, S.M. Heald, E.R. Weber, Acta Mater. 55 (2007) 6119.
[13] X. Zhang, D. Yang, R. Fan, J. Zhang, D. Que, J. Appl. Phys. 84 (1998) 5502.
[14] W. Wijaranakula, J. Appl. Phys. 79 (1996) 4450.